EEET ECOLOGICAL ENGINEERING & ENVIRONMENTAL TECHNOLOGY

Ecological Engineering & Environmental Technology, 2026, 27(10), 234–257
https://doi.org/10.12912/27197050/230933
ISSN 2719–7050, License CC-BY 4.0

Received: 2026.07.26
Accepted: 2026.08.31
Published: 2026.09.10

Roadside PM10 concentrations in relation to traffic volume and meteorological conditions in Makassar, Indonesia

Siti Nurafifah Asis[1], Sumarni Hamid Aly[1*], Muralia Hustim[1], Nurul Masyiah Rani Harusi[1], Muh. Khalil Jibran[1], Aisyah Handayani[1]

[1] Department of Environmental Engineering, Faculty of Engineering, University of Hasanuddin, Malino Str. km 6, Gowa Regency, Sulawesi Selatan, 92171, Indonesia
* Corresponding author's e-mail: marni_hamidaly@yahoo.com

ABSTRACT

This study aimed to quantify the combined influence of traffic activity and meteorological conditions on roadside PM_{10} in Makassar, Indonesia, and to evaluate whether an integrated model provides better predictive performance than traffic-only and nonlinear alternatives. Field measurements were conducted at 30 roadside points between 25 February and 20 March 2025. PM_{10} concentrations were measured using a high volume air sampler, traffic was represented by total vehicle volume, and temperature, relative humidity, air pressure, wind direction, and wind velocity were recorded concurrently. The analysis included the Shapiro–Wilk test, Pearson correlation, simple linear regression, multiple linear regression, fifth-order polynomial regression, Random Forest benchmarking, leave-one-out cross-validation, residual diagnostics, Moran's I, and exploratory inverse distance weighting. Total vehicle volume was positively associated with PM_{10} ($r = 0.752$, $p < 0.001$), while relative humidity showed a strong negative association ($r = -0.740$, $p < 0.001$). The final multiple linear regression model using total vehicle volume and relative humidity achieved $R^2 = 0.720$ and adjusted $R^2 = 0.699$. Under leave-one-out cross-validation, it outperformed the other models with RMSE = 24.79 μg/m³, MAE = 18.62 μg/m³, cross-validated $R^2 = 0.650$, and observed–predicted $r = 0.807$. Random Forest ranked second but did not surpass the multiple linear model. No significant global spatial autocorrelation was detected in measured PM_{10} or model residuals, and IDW showed weak out-of-location predictive skill, so the spatial surface was retained only as an exploratory visualization. The study is limited by 30 point-level observations, selected one-hour monitoring periods, and the absence of external seasonal validation. Practically, the model provides an interpretable screening framework for identifying roadside locations where traffic intensity and humidity jointly indicate elevated PM_{10}. Its originality lies in combining traffic, meteorology, internal validation, robustness diagnostics, a machine-learning benchmark, and explicitly constrained spatial interpretation within a single roadside assessment framework for Makassar.

Keywords: air pollution, inverse distance weighting, meteorological conditions, PM_{10}, roadside monitoring, traffic volume.

INTRODUCTION

Road transportation is an important source of particulate pollution in urban environments. Previous studies have shown that changes in traffic activity can substantially affect urban air quality, highlighting the importance of traffic-related particulate emissions (Piscitello et al., 2021; Harrison et al., 2021). Particulate matter with aerodynamic diameters of 10 μm or less (PM_{10}) is an important urban air-quality indicator because it can enter the respiratory system. Short-term and long-term exposure to particulate pollution has been associated with respiratory and cardiovascular effects and increased mortality risk, supporting the need for reliable monitoring in densely trafficked urban areas (Orellano et al., 2020; Dominski et al., 2021).

Makassar is a rapidly developing urban center in eastern Indonesia with intensive transport activity on its major roads. Motorized vehicles have been identified as relevant sources of PM_{10} and other pollutant emissions on urban road sections in Makassar (Savirah Nurul Auliah et al., 2023). A recent field study also reported that vehicle volume was associated with roadside PM_{10}, although traffic-only linear and polynomial models did not fully explain the observed variability (Aly et al., 2025).

Meteorological conditions influence the accumulation, transport, deposition, and removal of particulate matter. Wind velocity and direction regulate dispersion, while temperature and atmospheric stability influence vertical mixing. Relative humidity can affect hygroscopic growth, deposition, road-surface moisture, and dust resuspension. Roadside studies in Madrid and Bangkok have therefore emphasized that traffic-related particulate levels should be interpreted together with local meteorological conditions (Laña et al., 2016; Sahanavin et al., 2018). The relationships between particulate concentrations and meteorological parameters can vary among climates, locations, and observation periods. Evidence from Jakarta showed complex and location-specific interactions between air quality and meteorological conditions, while a recent study in Thailand reported a negative PM_{10} relationship with relative humidity and a positive relationship with air pressure (Istiana et al., 2023; Chaiprakarn et al., 2025). These differences emphasize the need for locally derived analyses rather than universal assumptions.

Statistical models can quantify empirical relationships between PM_{10} and potential predictors. Linear regression offers direct interpretation, whereas nonlinear models may represent curvature that cannot be described by a single linear term (Taheri Shahraiyni and Sodoudi, 2016). Model complexity should nevertheless be balanced against interpretability and generalization, particularly for limited datasets. Cross-validation provides a systematic approach for evaluating predictive performance on observations excluded during model fitting (James et al., 2021).

Spatial interpolation can extend point-based estimates into a continuous representation of pollutant distribution. Inverse distance weighting assigns greater influence to nearby observations and has been applied to particulate-matter mapping where monitoring data are spatially limited. However, an interpolated surface represents estimated spatial tendencies rather than direct measurements at unsampled locations (Choi and Chong, 2022). Previous roadside studies in Makassar have primarily focused on traffic volume as the sole predictor of PM_{10} and did not evaluate whether incorporating local meteorological conditions could substantially improve predictive performance or provide a more realistic representation of roadside particulate variability. Consequently, the combined influence of traffic activity and meteorological factors on roadside PM_{10} in Makassar remains insufficiently understood, and the predictive value of integrated statistical models has not been systematically assessed.

This study hypothesized that incorporating meteorological variables together with traffic volume would improve the explanation and prediction of roadside PM_{10} compared with traffic-only models. Accordingly, the aim of this study was to develop and validate an integrated statistical model describing roadside PM_{10} variability in Makassar by combining traffic and meteorological observations and to visualize the resulting spatial distribution.

MATERIALS AND METHODS

Study area and research design

Makassar is a coastal city and a major center of economic and transportation activity in eastern Indonesia. The study was conducted at 30 roadside measurement points distributed across its urban road network. The points represented roads with differing traffic intensity and surrounding urban conditions. Their spatial distribution is shown in Figure 1 and Table 1.

Field measurements were conducted from 25 February to 20 March 2025. The study used a quantitative field-based design integrating direct measurements, statistical analysis, regression modeling, internal validation, and spatial interpolation. Measurements were undertaken during four one-hour periods: 08:00–09:00, 13:00–14:00, 16:00–17:00, and 19:00–20:00 Central Indonesian Time. PM_{10}, traffic volume, and meteorological conditions were observed concurrently at each point. The overall design is presented in Figure 2.

Field measurements

PM_{10} measurement

PM_{10} concentrations were measured using a Staplex TFIA-2 High Volume Air Sampler (HVAS; Staplex, United States) with an

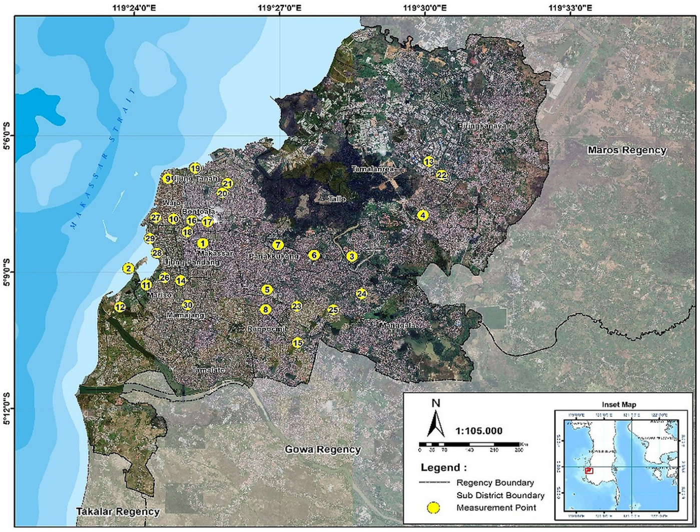

Figure 1. Research location

Table 1. Roadside measurement locations and coordinates

Point	Road/location	District	Longitude	Latitude
1	Jl. Veteran	Makassar	119.4235877	-5.1394779
2	Jl. Metro Tanjung Bunga	Tamalate	119.3980582	-5.1487355
3	Jl. Poros Makassar–Maros	Tamalanrea	119.4748838	-5.1442924
4	Jl. Bumi Tamalanrea Permai	Tamalanrea	119.4993053	-5.1291573
5	Jl. Boulevard	Panakkukang	119.4457089	-5.1564651
6	Jl. Urip Sumoharjo	Panakkukang	119.4619042	-5.1437853
7	Jl. Urip Sumoharjo	Panakkukang	119.4494929	-5.1400623
8	Jl. Hertasning	Rappocini	119.4452273	-5.1637286
9	Jl. Satando	Ujung Tanah	119.4116132	-5.1157853
10	Jl. HOS Cokroaminoto	Wajo	119.4135679	-5.1305929
11	Jl. Metro Tanjung Bunga	Mariso	119.4041764	-5.1547522
12	Jl. Metro Tanjung Bunga	Tamalate	119.3951422	-5.1628491
13	Jl. Kima IV	Biringkanaya	119.5014343	-5.1095362
14	Jl. Ratulangi	Mamajang	119.4160831	-5.1530833
15	Jl. Aroepala	Rappocini	119.4562551	-5.1759492
16	Jl. Mesjid Raya	Bontoala	119.4198169	-5.1310917
17	Jl. Pasar Terong	Bontoala	119.4252232	-5.1315890
18	Jl. G. Bawakaraeng	Makassar	119.4182629	-5.1353578
19	Jl. Sabutung	Ujung Tanah	119.4210446	-5.1120043
20	Jl. Sunu	Tallo	119.4303212	-5.1210043
21	Jl. Teuku Umar	Tallo	119.4321569	-5.1175675
22	Jl. Niga Daya Ruko	Biringkanaya	119.5057735	-5.1144649
23	Jl. Toddopuli Raya Timur	Manggala	119.4558960	-5.1625705
24	Jl. AMD	Manggala	119.4782310	-5.1579480
25	Jl. Ujung Bori	Manggala	119.4684456	-5.1639003
26	Jl. Rajawali	Mariso	119.4105079	-5.1520537
27	Jl. Sulawesi	Wajo	119.4074245	-5.1300303
28	Jl. Penghibur	Ujung Pandang	119.4078634	-5.1430010
29	Jl. Penghibur	Ujung Pandang	119.4054457	-5.1377269
30	Jl. Landak Lama	Mamajang	119.4184472	-5.1620691

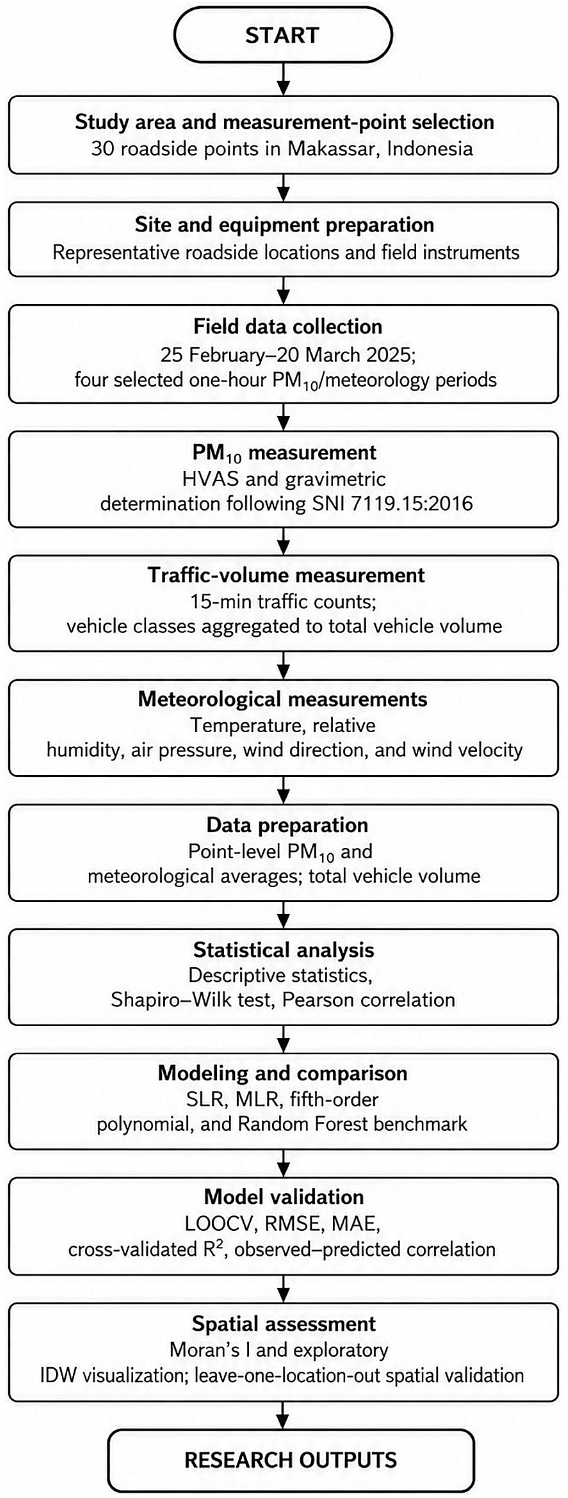

Figure 2. Research design of the study

11-cm-diameter Whatman GF/A glass microfiber filter. The HVAS was operated for 60 min during each measurement period at an operational flow rate of 1.1–1.7 m^3/min. The flow rate was recorded every three minutes. The inlet was positioned at least 2 m above ground level in accordance with the sampling placement requirements of SNI 7119.15:2016. Filters were handled using forceps and gloves and protected with labeled aluminum foil. Filter mass was determined using a CONTROLS electronic analytical balance with a readability of 0.0001 g. Each filter was weighed three times, and the mean value was used for gravimetric PM_{10} determination. Standard flow rate, standard air volume, and PM_{10} concentration were calculated using Equations 1–3.

$$Q_s = Q_a \frac{P_a}{P_s}\frac{T_s}{T_a} \tag{1}$$

$$V_{std} = \frac{\Sigma\, Q_{s,i}}{n}\, t \tag{2}$$

$$C_{PM_{10}} = \frac{(W_2 - W_1)\,\times\,10^6}{V_{std}} \tag{3}$$

where: Q_s and Q_a are the standard and actual flow rates; P_a and P_s are the actual and standard pressures; T_a and T_s are the actual and standard absolute temperatures; V_{std} is the standard air volume; n is the number of flow-rate readings; t is the sampling duration; and W_1 and W_2 are the filter masses before and after sampling, respectively.

Traffic volume measurement

Traffic data were collected at 30 points using the Multi Counter application. Vehicles were recorded as motorcycles, light vehicles, and heavy vehicles. Counts were conducted for 15 min during each observation hour from 07:00 to 20:15 Central Indonesian Time (WITA). Intervals from 07:00–10:15 were grouped as morning, 11:00–14:15 as midday, 15:00–18:15 as afternoon, and 19:00–20:15 as evening. Vehicle-class composition was retained in Supplementary Table S2, whereas total vehicle volume was used as the principal traffic predictor.

$$V_j = MC_j + LV_j + HV_j \tag{4}$$

$$\begin{gathered} V_{total} = V_{pagi} + V_{siang} + \\ + V_{sore} + V_{malam} \end{gathered} \tag{5}$$

where: V_j is the total number of vehicles in time group j, whereas MC, LV, and HV denote motorcycles, light vehicles, and heavy vehicles, respectively. Equation 5 yields the total vehicle volume per measurement point used in the analysis.

Meteorological measurements

Air temperature, relative humidity, air pressure, wind direction, and wind velocity were measured using an Ambient Weather WS-2000 automatic weather station. Measurements were recorded every five minutes during each one-hour PM_{10} period, averaged to obtain one value per period, and then averaged across the four periods to obtain the point-level value. Air pressure is retained in the source-data unit of mmHg. general measurement principles described by the World Meteorological Organization (2021).

Measurement instruments and documentation

The main instruments, specifications, functions, and operational conditions are summarized in Table 2 and Figure 3 to improve measurement reproducibility.

Data analysis

Field data were aggregated to obtain one representative value for each of the 30 roadside measurement points. PM_{10} concentrations and meteorological variables from the four selected one-hour periods were averaged at the point level, whereas traffic activity was represented by the total vehicle volume accumulated over the monitored traffic-counting periods. The resulting analytical dataset therefore consisted of 30 point-level observations. These point-level PM_{10} means represent the four selected observation periods and should not be interpreted as 24-h averages.

Normality was assessed using the Shapiro–Wilk test at a significance level of 0.05. A p-value greater than 0.05 was interpreted as no statistically significant departure from normality (Mishra et al., 2019). Pearson correlation analysis was subsequently applied to evaluate the direction and strength of the associations between PM_{10} and total vehicle volume, temperature, relative humidity, air pressure, wind direction, and wind velocity. Correlation coefficients were interpreted as measures of statistical association rather than evidence of causality (Schober et al., 2018).

Predictor selection considered correlation magnitude, environmental relevance, sample size, and model parsimony. Total vehicle volume was retained as the traffic-related predictor. Relative humidity was selected as the meteorological predictor because it exhibited the largest absolute meteorological correlation with PM_{10} and provided a process-based interpretation through particle deposition, surface moisture, and road-dust resuspension. Road-dust resuspension is influenced by meteorological and road-surface conditions, supporting the environmental relevance of relative humidity in roadside particulate analysis (Rienda and Alves, 2021). Air pressure was retained in the correlation analysis as a contextual meteorological correlate but was not entered into the final parsimonious two-predictor model.

Regression modeling and comparison

Four modeling approaches were evaluated: simple linear regression (SLR), multiple linear regression (MLR), exploratory fifth-order polynomial regression, and Random Forest regression as a nonlinear machine-learning benchmark. The Random Forest benchmark used the same two predictors as the MLR model to permit a consistent comparison.

Table 2. Instruments and materials used for field and laboratory measurements

No.	Instrument/Material	Brand/Model/Specification	Function	Operational information
1	High volume air sampler	Staplex TFIA-2	PM_{10} sampling	60 min; 1,1-1,7 m³/min; inlet ≥2 m; SNI 7119.15:2016.
2	Glass microfiber filter	Whatman GF/A; 11 cm; nominal pore size 1,6 μm	PM_{10} collection medium	Labeled, handled with forceps/gloves, and protected with aluminum foil.
3	Analytical balance	CONTROLS; readability 0,0001 g	Filter mass determination	Three replicate weighings; the mean value was used for PM_{10} gravimetry.
4	Automatic weather station	Ambient Weather WS-2000	Meteorological measurements	Temperature, relative humidity, air pressure, wind direction, and wind velocity every 5 min.
5	Multi counter application	Digital traffic-counting application	Vehicle counting	15-min counts by motorcycle, light vehicle, and heavy vehicle.
6	Supporting equipment	tripod, pinset, aluminium foil, zipper, sarung tangan, kabel rol	Instrument placement and filter handling	Maintains instrument stability and filter identity and minimizes contamination.

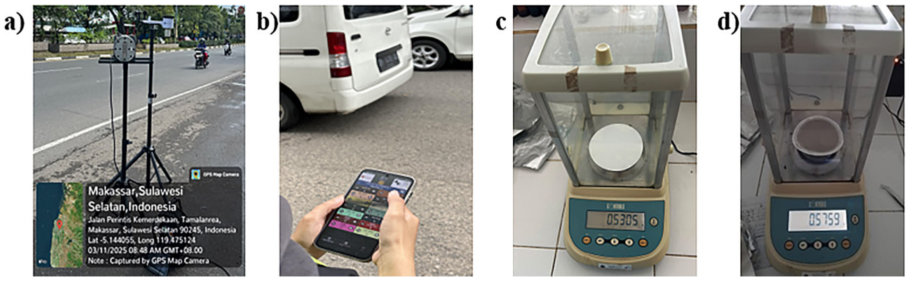

Figure 3. Documentation of roadside measurements and PM_{10} gravimetric analysis: (a) roadside instrument placement; (b) traffic counting using the Multi Counter application; (c) initial filter weighing before sampling; and (d) final filter weighing after sampling

The simple linear regression model was expressed as:

$$Y = \beta_0 + \beta_1 X + \varepsilon \quad (6)$$

where: Y is PM_{10} concentration, X is total vehicle volume, β_0 is the intercept, β_1 is the regression coefficient, and ε is the error term.

The multiple linear regression model was expressed as:

$$Y = \beta_0 + \beta_1 X_1 + \beta_2 X_2 + \varepsilon \quad (7)$$

where: Y is PM_{10} concentration, X_1 represents total vehicle volume and X_2 represents relative humidity, and ε is the error term.

The exploratory fifth-order polynomial regression model was expressed as:

$$Y = \beta_0 + \beta_1 X + \beta_2 X^2 + + \beta_3 X^3 + \beta_4 X^4 + \beta_5 X^5 + \varepsilon \quad (8)$$

The fifth-order polynomial was retained only as an exploratory nonlinear traffic-only comparison. Because increasingly flexible models may show improved in-sample fit while generalizing poorly, its performance was evaluated using information criteria and cross-validation rather than fitted R^2 alone (James et al., 2021).

Random Forest regression was additionally evaluated as a modern nonlinear benchmark because an ensemble of randomized regression trees can represent nonlinear relationships and interactions without prespecifying a single functional form (Scornet et al., 2015). The model used total vehicle volume and relative humidity, 300 regression trees, a minimum leaf size of 3, max_features = 1.0, and random_state = 20260806. No extensive hyperparameter optimization was performed because the dataset contained only 30 point-level observations. Random Forest was therefore treated as a comparative benchmark rather than the primary model. Before fitting the MLR model, multicollinearity was evaluated using tolerance and the variance inflation factor (VIF). Tolerance values above 0.10 and VIF values below 10 were used to screen for problematic multicollinearity (Kim, 2019). For the MLR model, unstandardized coefficients, standard errors, standardized regression coefficients, p-values, 95% confidence intervals, and HC3 heteroscedasticity-consistent inference were reported to evaluate predictor significance and coefficient robustness. HC3 is particularly useful as a conservative robust standard-error approach in small samples or in the presence of leverage (Mansournia et al., 2021). Model comparison considered fitted R^2, adjusted R^2, Akaike Information Criterion (AIC), Bayesian Information Criterion (BIC), predictive performance, parsimony, and environmental interpretability.

Model validation and diagnostic assessment

All four models were evaluated using leave-one-out cross-validation (LOOCV). In each iteration, one measurement point was excluded, the model was fitted using the remaining 29 observations, and the excluded observation was predicted. This process was repeated until each of the 30 points had served once as the validation observation. LOOCV was treated as internal predictive validation rather than external validation (James et al., 2021). Predictive error was quantified using root mean square error (RMSE):

$$RMSE = \sqrt{\frac{1}{n}\sum_{i=1}^{n}(y_i - \hat{y}_i)^2} \quad (9)$$

Mean absolute error (MAE):

$$MAE = \frac{1}{n}\sum_{i=1}^{n}|y_i - \hat{y}_i| \qquad (10)$$

and the cross-validated coefficient of determination:

$$R^2_{CV} = 1 - \frac{\sum_{i=1}^{n}(y_i - \hat{y}_i)^2}{\sum_{i=1}^{n}(y_i - \bar{y})^2} \qquad (11)$$

where: y_i is the observed PM_{10} concentration, $\hat{y}_i$ is the prediction obtained when observation i was excluded from model fitting, $\bar{y}$ is the mean observed PM_{10} concentration, and n = 30. T

he Pearson correlation coefficient between observed and LOOCV-predicted concentrations was also calculated. Lower RMSE and MAE and higher R^2_{CV} and observed–predicted correlation indicate better predictive agreement.

For the selected MLR model, residual robustness was additionally assessed. Residual normality was examined using the Shapiro–Wilk test, heteroscedasticity using the Breusch–Pagan and White tests, and potentially influential observations using Cook's distance. HC3 robust inference was used as an additional coefficient-robustness check (Mansournia et al., 2021).

Spatial autocorrelation and exploratory IDW visualization

Because the observations were geographically distributed, spatial autocorrelation was assessed before interpreting the spatial visualization. Global Moran's I was calculated for both measured PM_{10} concentrations and MLR residuals, with statistical significance evaluated using 999 permutations. Moran's I provides a global measure of spatial autocorrelation and is useful for assessing whether similar values exhibit systematic spatial organization rather than spatial randomness (Chen, 2023). Moran's I for measured PM_{10} was used to examine spatial structure in the observations, whereas Moran's I for the MLR residuals was used to determine whether spatial structure remained after accounting for total vehicle volume and relative humidity.

The selected MLR model was subsequently used to generate point-level PM_{10} estimates at the 30 monitored locations. These estimates were visualized using inverse distance weighting (IDW). IDW was retained because the spatial component of this study was intended to provide a transparent and reproducible visualization of relative variation among monitored roadside locations rather than an independently validated city-wide geostatistical forecasting model. IDW has been used for particulate-matter mapping, and cross-validation is important for evaluating the reliability of interpolated PM surfaces (Shukla et al., 2020; Choi and Chong, 2022).

The IDW estimator was expressed as:

$$\hat{Z}(x_0) = \frac{\sum_{i=1}^{n} d_i^{-p} Z(x_i)}{\sum_{i=1}^{n} d_i^{-p}} \qquad (12)$$

where: $\hat{Z}(x_0)$ is the estimated value at location x_0, $Z(x_i)$ is the model-estimated PM_{10} concentration at monitored point i, d_i is the distance between point i and the location being estimated, and p is the distance-decay power.

Candidate powers of $p = 1$, $p = 2$ and $p = 3$ were evaluated using leave-one-location-out spatial validation. In each iteration, one monitored location was removed and its value was estimated using the remaining 29 locations. Spatial validation performance was assessed using RMSE, MAE, cross-validated R^2, and observed–predicted correlation. The power producing the lowest validation error was retained for the exploratory visualization. In the final analysis, $p = 1$ produced the lowest leave-one-location-out error among the tested powers. Because spatial cross-validation indicated limited predictive performance at omitted locations, the resulting IDW surface was interpreted strictly as an exploratory visualization of relative spatial tendencies and not as a direct measurement or validated prediction at unsampled roads.

RESULTS

Roadside PM_{10}, traffic, and meteorological characteristics

PM_{10} concentrations

PM_{10} measurements were analyzed descriptively to characterize concentration variability across measurement points and observation periods. The PM_{10} values were also descriptively compared with the Indonesian ambient-air quality standard of 75 µg/m³ established in Government Regulation of the Republic of Indonesia Number 22 of 2021. This comparison was used only as an initial indication because the regulatory value refers to a 24-h average, whereas the present study measured four selected one-hour periods (Table 3).

Figure 4 presents the point-level PM_{10} concentrations. Values ranged from 93.63 to 257.99 μg/m³. The highest concentration occurred at Point 3, whereas the lowest occurred at Point 14, demonstrating substantial spatial variation among the monitored roadside locations.

All point-level concentrations were numerically higher than the Indonesian 24-h ambient-air standard of 75 μg/m³ (Government of the Republic of Indonesia, 2021). This comparison does not establish formal non-compliance because the measurements represented selected one-hour periods rather than continuous 24-h averages. The results instead indicate elevated roadside conditions during the monitored periods.

Vehicle volume

Traffic was observed in three vehicle classes: motorcycles (MC), light vehicles (LV), and heavy vehicles (HV). These classes were used to describe traffic composition at each measurement point in Makassar.

Vehicle data were collected using the Multi Counter application at the 30 observation points. Counts were conducted for 15 min during each

Table 3. PM_{10} concentrations at the 30 roadside measurement points

Measurement point	Road name	Morning (08.00–09.00) WITA	Midday (12.00–13.00) WITA	Afternoon (15.30–16.30) WITA	Evening (19.00–20.00)	Mean PM_{10}	Reference standard
1	Jl. Veteran	59.11	131.16	375.43	312.89	219.65	75
2	Jl. Metro Tanjung Bunga	316.78	232.95	87.08	31.84	167.16	75
3	Jl. Poros Makassar–Maros	251.79	277.26	344.14	158.78	257.99	75
4	Jl. Bumi Tamalanrea Permai	150.05	152.83	223.44	242.51	192.21	75
5	Jl. Boulevard	27.16	319.25	364.39	228.02	234.71	75
6	Jl. Urip Sumoharjo	42.42	176.00	414.33	104.02	184.19	75
7	Jl. Urip Sumoharjo	169.30	274.64	335.38	228.57	251.97	75
8	Jl. Hertasning	257.23	51.86	236.28	48.51	148.47	75
9	Jl. Satando	141.93	130.94	290.49	247.11	202.62	75
10	Jl. HOS Cokroaminoto	145.27	116.06	49.58	121.22	108.03	75
11	Jl. Metro Tanjung Bunga	299.91	367.94	118.96	132.21	229.76	75
12	Jl. Metro Tanjung Bunga	280.47	215.93	187.71	112.76	199.22	75
13	Jl. Kima IV	220.64	392.17	144.00	43.74	200.14	75
14	Jl. Ratulangi	71.37	17.18	165.21	120.74	93.63	75
15	Jl. Aroepala	202.52	145.69	345.00	48.51	185.43	75
16	Jl. Mesjid Raya	141.80	124.64	295.81	34.41	149.17	75
17	Jl. Pasar Terong	277.22	345.78	161.05	149.39	233.36	75
18	Jl. G. Bawakaraeng	170.30	372.25	219.31	112.82	218.67	75
19	Jl. Sabutung	135.28	363.88	182.17	231.41	228.19	75
20	Jl. Sunu	27.58	151.23	265.97	121.11	141.47	75
21	Jl. Teuku Umar	240.50	229.48	396.81	136.27	250.77	75
22	Jl. Niga Daya Ruko	4.94	52.09	99.56	314.53	117.78	75
23	Jl. Toddopuli Raya Timur	81.51	71.79	208.89	360.76	180.74	75
24	Jl. AMD	293.72	281.38	313.60	51.34	235.01	75
25	Jl. Ujung Bori	296.81	37.00	360.68	151.69	211.55	75
26	Jl. Rajawali	234.47	88.72	283.62	279.44	221.56	75
27	Jl. Sulawesi	223.96	162.28	175.66	184.84	186.69	75
28	Jl. Penghibur	68.53	177.24	262.54	223.45	182.94	75
29	Jl. Penghibur	61.30	301.53	210.63	314.94	222.10	75
30	Jl. Landak Lama	418.48	118.59	84.19	145.41	191.67	75

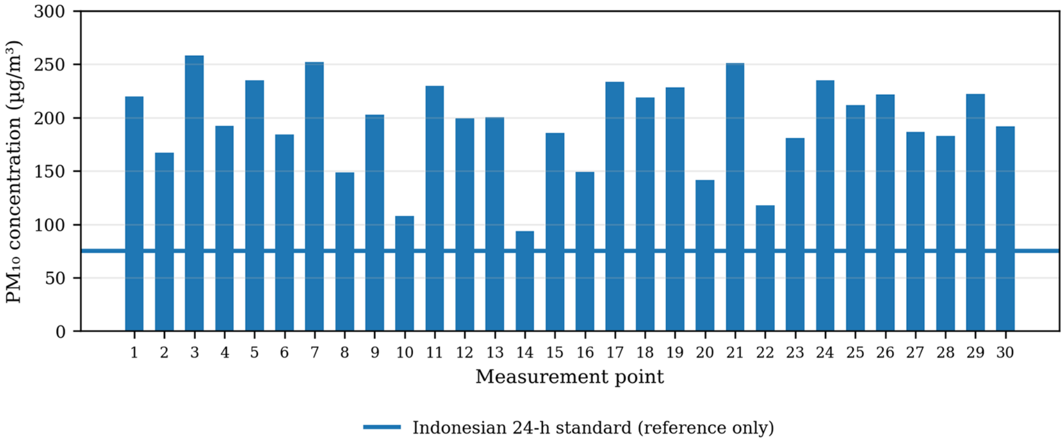

Figure 4. Average PM_{10} concentrations across the measurement points

observation hour at 07:00–07:15, 08:00–08:15, 09:00–09:15, 10:00–10:15, 11:00–11:15, 12:00–12:15, 13:00–13:15, 14:00–14:15, 15:00–15:15, 16:00–16:15, 17:00–17:15, 18:00–18:15, 19:00–19:15, and 20:00–20:15 WITA.

During each interval, passing vehicles were recorded by class. The counts were then summarized to determine traffic volume at each measurement point and observation interval. These data were used to characterize traffic composition and to support analysis of the relationship between total vehicle volume and PM_{10} concentration (Table 4).

Total vehicle volume ranged from 5,472 vehicles/4 h at Point 20 to 22,788 vehicles/4 h at Point 18 (Figure 5), indicating substantial differences in traffic activity among the monitored roads. Point 18, which had the greatest traffic volume, did not correspond to Point 3, where the highest PM_{10} concentration was observed. The mismatch between the locations of the maximum traffic volume and maximum PM_{10} illustrates that traffic activity was important but did not independently determine roadside concentration. Traffic contributes particles through exhaust emissions, brake and tire wear, road-surface abrasion, and dust resuspension, while the resulting concentration is further modified by local meteorology and roadside conditions (Piscitello et al., 2021; Rienda and Alves, 2021).

Meteorological conditions

The meteorological variables measured in this study were air temperature, relative humidity, air pressure, wind direction, and wind velocity. Meteorological measurements were conducted concurrently with PM_{10} sampling during four periods: 08:00–09:00, 13:00–14:00, 16:00–17:00, and 19:00–20:00 WITA.

Meteorological data were recorded every five minutes during each measurement period. The readings were averaged to obtain one value for each meteorological parameter within each observation period. These data were used to characterize atmospheric conditions relevant to pollutant dispersion, dilution, deposition, and accumulation around the measurement points (Table 5).

Meteorological conditions varied across the 30 measurement points (Figure 6). Temperature ranged from 28.42 to 32.56 °C, relative humidity from 59.02 to 81.06%, air pressure from 1005.97 to 1010.14 hPa, wind direction from 128.56 to 230.74°, and wind velocity from 0.12 to 2.64 m/s.

Low wind velocities at several points may have limited pollutant dilution and favored local accumulation. Differences in relative humidity may also have altered particle deposition and road-surface moisture, thereby influencing resuspension. Roadside PM_{10} should therefore be interpreted through the combined influence of source activity and atmospheric conditions.

Environmental relationships influencing roadside PM_{10}

The Shapiro–Wilk test was applied before parametric analysis. The results are presented in Table 6. All p-values exceeded 0.05, supporting the use of Pearson correlation to examine the point-level linear relationships. Table 7 summarizes the correlation coefficients.

Table 4. Traffic volume and vehicle-class composition at the 30 measurement points

Measurement point	Road name	Interval	Vehicle class			Total vehicle volume per point
			MC	LV	HV	
1	Jl. Veteran	Morning	2129	728	204	13310
		Midday	2293	859	242	
		Afternoon	2509	889	262	
		Evening	2191	760	244	
2	Jl. Metro Tanjung Bunga	Morning	1667	499	33	9561
		Midday	1800	590	48	
		Afternoon	1967	610	52	
		Evening	1717	521	57	
3	Jl. Poros Makassar–Maros	Morning	3534	1011	69	20063
		Midday	3816	1198	102	
		Afternoon	4170	1237	110	
		Evening	3640	1055	121	
4	Jl. Bumi Tamalanrea Permai	Morning	3118	748	449	18763
		Midday	3362	901	522	
		Afternoon	3677	920	563	
		Evening	3209	781	513	
5	Jl. Boulevard	Morning	3621	1318	45	21668
		Midday	3904	1544	77	
		Afternoon	4270	1605	84	
		Evening	3726	1375	99	
6	Jl. Urip Sumoharjo	Morning	2629	1115	64	16557
		Midday	2831	1300	91	
		Afternoon	3098	1356	99	
		Evening	2704	1164	106	
7	Jl. Urip Sumoharjo	Morning	3035	1163	309	19595
		Midday	3265	1365	367	
		Afternoon	3575	1418	396	
		Evening	3119	1213	370	
8	Jl. Hertasning	Morning	1537	509	234	9912
		Midday	1653	602	273	
		Afternoon	1810	622	294	
		Evening	1579	531	268	
9	Jl. Satando	Morning	2409	815	371	15631
		Midday	2591	963	432	
		Afternoon	2837	996	466	
		Evening	2476	850	425	
10	Jl. HOS Cokroaminoto	Morning	1872	415	218	10891
		Midday	2019	502	256	
		Afternoon	2208	511	276	
		Evening	1927	433	254	
11	Jl. Metro Tanjung Bunga	Morning	3616	1325	168	22214
		Midday	3896	1554	215	
		Afternoon	4263	1615	231	
		Evening	3720	1382	229	

Table 4. Cont. Traffic volume and vehicle-class composition at the 30 measurement points

12	Jl. Metro Tanjung Bunga	Morning	2523	952	53	15340
		Midday	2719	1114	79	
		Afternoon	2974	1159	85	
		Evening	2596	994	92	
13	Jl. Kima IV	Morning	2104	813	157	13365
		Midday	2264	953	191	
		Afternoon	2478	990	207	
		Evening	2163	849	196	
14	Jl. Ratulangi	Morning	1687	418	426	11004
		Midday	1814	505	487	
		Afternoon	1987	515	524	
		Evening	1734	436	471	
15	Jl. Aroepala	Morning	1528	536	245	10039
		Midday	1643	633	284	
		Afternoon	1800	655	306	
		Evening	1571	559	279	
16	Jl. Mesjid Raya	Morning	918	329	111	5903
		Midday	988	387	130	
		Afternoon	1081	401	141	
		Evening	944	343	130	
17	Jl. Pasar Terong	Morning	2935	922	142	17385
		Midday	3165	1088	180	
		Afternoon	3461	1126	194	
		Evening	3020	962	190	
18	Jl. G. Bawakaraeng	Morning	3725	1446	70	22788
		Midday	4014	1691	106	
		Afternoon	4391	1761	115	
		Evening	3832	1509	128	
19	Jl. Sabutung	Morning	2427	676	406	15258
		Midday	2614	808	469	
		Afternoon	2861	829	506	
		Evening	2497	706	459	
20	Jl. Sunu	Morning	882	281	96	5472
		Midday	949	333	113	
		Afternoon	1039	344	122	
		Evening	907	293	113	
21	Jl. Teuku Umar	Morning	2689	1083	346	17903
		Midday	2889	1269	407	
		Afternoon	3165	1319	439	
		Evening	2763	1130	404	
22	Jl. Niga Daya Ruko	Morning	1503	447	30	8607
		Midday	1623	528	44	
		Afternoon	1774	546	47	
		Evening	1547	466	52	
23	Jl. Toddopuli Raya Timur	Morning	1815	686	243	11931
		Midday	1951	806	285	
		Afternoon	2137	837	307	
		Evening	1865	716	283	

Table 4. Cont. Traffic volume and vehicle-class composition at the 30 measurement points

24	Jl. AMD	Morning	3406	1324	56	20809
		Midday	3670	1548	88	
		Afternoon	4015	1612	95	
		Evening	3505	1382	108	
25	Jl. Ujung Bori	Morning	3357	829	63	18476
		Midday	3627	989	95	
		Afternoon	3963	1016	102	
		Evening	3459	865	111	
26	Jl. Rajawali	Morning	2133	722	530	14718
		Midday	2289	857	607	
		Afternoon	2509	883	655	
		Evening	2190	753	590	
27	Jl. Sulawesi	Morning	1400	608	133	9307
		Midday	1504	709	160	
		Afternoon	1647	739	173	
		Evening	1438	634	162	
28	Jl. Penghibur	Morning	1728	583	226	11029
		Midday	1859	688	265	
		Afternoon	2035	712	286	
		Evening	1776	608	263	
29	Jl. Penghibur	Morning	2147	589	268	13059
		Midday	2313	703	314	
		Afternoon	2530	722	339	
		Evening	2208	615	311	
30	Jl. Landak Lama	Morning	2131	858	333	14444
		Midday	2289	1006	388	
		Afternoon	2508	1045	419	
		Evening	2189	895	383	

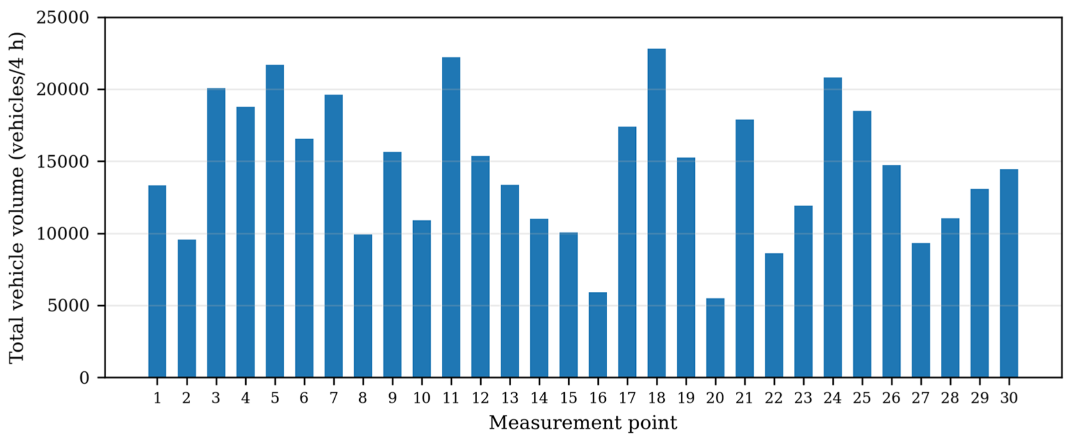

Figure 5. Total vehicle volume across the measurement points

Total vehicle volume showed a strong positive association with PM_{10} ($r = 0.752$, $p = 1.65 \times 10^{-6}$), whereas relative humidity showed a strong negative association ($r = -0.740$, $p = 2.95\times10^{-6}$). Air pressure was also strongly correlated ($r = 0.730$, $p = 4.72 \times 10^{-6}$), but was retained as a contextual bivariate correlate rather than added to the parsimonious two-predictor model. These correlations are associations and do not establish causal effects.

Table 5. Meteorological conditions at the 30 measurement points

Measurement point	Road name	Interval	Meteorological variables					Mean meteorological values				
			Temperature (°C)	Relative humidity (%)	Air pressure (mmHg)	Wind direction (°)	Wind velocity (m/s)	Temperature (°C)	Relative humidity (%)	Air pressure (mmHg)	Wind direction (°)	Wind velocity (m/s)
1	Jl. Veteran	Morning	29.1	68.93	756.81	195.82	1.82	29.45	67.53	756.69	203.82	1.82
		Midday	30.3	65.43	756.63	209.82	1.75					
		Afternoon	29.6	67.83	756.61	212.82	1.91					
		Evening	28.8	67.93	756.71	196.82	1.8					
2	Jl. Metro Tanjung Bunga	Morning	32.14	72.9	755.72	176.16	1.31	32.49	71.5	755.6	184.16	1.31
		Midday	33.34	69.4	755.54	190.16	1.24					
		Afternoon	32.64	71.8	755.52	193.16	1.4					
		Evening	31.84	71.9	755.62	177.16	1.29					
3	Jl. Poros Makassar–Maros	Morning	31.18	61.84	757.14	202.27	1.64	31.53	60.44	757.02	210.27	1.64
		Midday	32.38	58.34	756.96	216.27	1.57					
		Afternoon	31.68	60.74	756.94	219.27	1.73					
		Evening	30.88	60.84	757.04	203.27	1.62					
4	Jl. Bumi Tamalanrea Permai	Morning	28.8	62.26	756.41	184.12	0.92	29.15	60.86	756.29	192.12	0.92
		Midday	30	58.76	756.23	198.12	0.85					
		Afternoon	29.3	61.16	756.21	201.12	1.01					
		Evening	28.5	61.26	756.31	185.12	0.9					
5	Jl. Boulevard	Morning	30.02	74.54	757.05	187.14	2.07	30.37	73.14	756.93	195.14	2.07
		Midday	31.22	71.04	756.87	201.14	2					
		Afternoon	30.52	73.44	756.85	204.14	2.16					
		Evening	29.72	73.54	756.95	188.14	2.05					
6	Jl. Urip Sumoharjo	Morning	32.21	78.36	756.3	221.63	1.39	32.56	76.96	756.18	229.63	1.39
		Midday	33.41	74.86	756.12	235.63	1.32					
		Afternoon	32.71	77.26	756.1	238.63	1.48					
		Evening	31.91	77.36	756.2	222.63	1.37					
7	Jl. Urip Sumoharjo	Morning	32.01	63.05	756.58	120.56	1.67	32.36	61.65	756.46	128.56	1.67
		Midday	33.21	59.55	756.4	134.56	1.6					
		Afternoon	32.51	61.95	756.38	137.56	1.76					
		Evening	31.71	62.05	756.48	121.56	1.65					
8	Jl. Hertasning	Morning	28.97	81.02	755.38	152.62	1.12	29.32	79.62	755.26	160.62	1.12
		Midday	30.17	77.52	755.2	166.62	1.05					
		Afternoon	29.47	79.92	755.18	169.62	1.21					
		Evening	28.67	80.02	755.28	153.62	1.1					
9	Jl. Satando	Morning	30.86	71.81	756.23	122.09	1.63	31.21	70.41	756.11	130.09	1.63
		Midday	32.06	68.31	756.05	136.09	1.56					
		Afternoon	31.36	70.71	756.03	139.09	1.72					
		Evening	30.56	70.81	756.13	123.09	1.61					
10	Jl. HOS Cokroaminoto	Morning	28.77	80.84	755.46	222.61	0.63	29.12	79.44	755.34	230.61	0.63
		Midday	29.97	77.34	755.28	236.61	0.56					
		Afternoon	29.27	79.74	755.26	239.61	0.72					
		Evening	28.47	79.84	755.36	223.61	0.61					
11	Jl. Metro Tanjung Bunga	Morning	29.9	72	756.97	203.78	0.57	30.25	70.6	756.85	211.78	0.57
		Midday	31.1	68.5	756.79	217.78	0.5					
		Afternoon	30.4	70.9	756.77	220.78	0.66					
		Evening	29.6	71	756.87	204.78	0.55					

Table 5. Cont. Meteorological conditions at the 30 measurement points

Measurement point	Road name	Interval	Meteorological variables					Mean meteorological values				
			Temperature (°C)	Relative humidity (%)	Air pressure (mmHg)	Wind direction (°)	Wind velocity (m/s)	Tempera-ture (°C)	Relative humidity (%)	Air pressure (mmHg)	Wind direction (°)	Wind velocity (m/s)
12	Jl. Metro Tanjung Bunga	Morning	31.2	70.1	756.36	172.44	0.66	31.55	68.7	756.24	180.44	0.66
		Midday	32.4	66.6	756.18	186.44	0.59					
		Afternoon	31.7	69	756.16	189.44	0.75					
		Evening	30.9	69.1	756.26	173.44	0.64					
13	Jl. Kima IV	Morning	31.26	69.54	756.77	169.63	0.76	31.61	68.14	756.65	177.63	0.76
		Midday	32.46	66.04	756.59	183.63	0.69					
		Afternoon	31.76	68.44	756.57	186.63	0.85					
		Evening	30.96	68.54	756.67	170.63	0.74					
14	Jl. Ratulangi	Morning	31.45	81.9	755.2	165.66	0.88	31.8	80.5	755.08	173.66	0.88
		Midday	32.65	78.4	755.02	179.66	0.81					
		Afternoon	31.95	80.8	755	182.66	0.97					
		Evening	31.15	80.9	755.1	166.66	0.86					
15	Jl. Aroepala	Morning	32	74.24	756.05	193.84	2.19	32.35	72.84	755.93	201.84	2.19
		Midday	33.2	70.74	755.87	207.84	2.12					
		Afternoon	32.5	73.14	755.85	210.84	2.28					
		Evening	31.7	73.24	755.95	194.84	2.17					
16	Jl. Mesjid Raya	Morning	29.8	76.78	755.28	222.74	1.98	30.15	75.38	755.16	230.74	1.98
		Midday	31	73.28	755.1	236.74	1.91					
		Afternoon	30.3	75.68	755.08	239.74	2.07					
		Evening	29.5	75.78	755.18	223.74	1.96					
17	Jl. Pasar Terong	Morning	28.07	68.98	757.52	144.53	1.66	28.42	67.58	757.4	152.53	1.66
		Midday	29.27	65.48	757.34	158.53	1.59					
		Afternoon	28.57	67.88	757.32	161.53	1.75					
		Evening	27.77	67.98	757.42	145.53	1.64					
18	Jl. G. Bawakaraeng	Morning	28.48	67.2	756.1	134.63	0.48	28.83	65.8	755.98	142.63	0.48
		Midday	29.68	63.7	755.92	148.63	0.41					
		Afternoon	28.98	66.1	755.9	151.63	0.57					
		Evening	28.18	66.2	756	135.63	0.46					
19	Jl. Sabutung	Morning	29.98	67.71	756.96	158.3	0.99	30.33	66.31	756.84	166.3	0.99
		Midday	31.18	64.21	756.78	172.3	0.92					
		Afternoon	30.48	66.61	756.76	175.3	1.08					
		Evening	29.68	66.71	756.86	159.3	0.97					
20	Jl. Sunu	Morning	29.23	74.21	756.38	144.51	2.39	29.58	72.81	756.26	152.51	2.39
		Midday	30.43	70.71	756.2	158.51	2.32					
		Afternoon	29.73	73.11	756.18	161.51	2.48					
		Evening	28.93	73.21	756.28	145.51	2.37					
21	Jl. Teuku Umar	Morning	30.61	67.95	757.07	214.09	1.71	30.96	66.55	756.95	222.09	1.71
		Midday	31.81	64.45	756.89	228.09	1.64					
		Afternoon	31.11	66.85	756.87	231.09	1.8					
		Evening	30.31	66.95	756.97	215.09	1.69					
22	Jl. Niga Daya Ruko	Morning	29.46	82.46	755.94	186.81	2.52	29.81	81.06	755.82	194.81	2.52
		Midday	30.66	78.96	755.76	200.81	2.45					
		Afternoon	29.96	81.36	755.74	203.81	2.61					
		Evening	29.16	81.46	755.84	187.81	2.5					

Table 5. Cont. Meteorological conditions at the 30 measurement points

Measurement point	Road name	Interval	Meteorological variables					Mean meteorological values				
			Temperature (°C)	Relative humidity (%)	Air pressure (mmHg)	Wind direction (°)	Wind velocity (m/s)	Tempera-ture (°C)	Relative humidity (%)	Air pressure (mmHg)	Wind direction (°)	Wind velocity (m/s)
23	Jl. Toddopuli Raya Timur	Morning	31.13	74.72	754.66	176.34	1.18	31.48	73.32	754.54	184.34	1.18
		Midday	32.33	71.22	754.48	190.34	1.11					
		Afternoon	31.63	73.62	754.46	193.34	1.27					
		Evening	30.83	73.72	754.56	177.34	1.16					
24	Jl. AMD	Morning	31.96	68.79	757.2	191.58	0.12	32.31	67.39	757.08	199.58	0.12
		Midday	33.16	65.29	757.02	205.58	0.05					
		Afternoon	32.46	67.69	757	208.58	0.21					
		Evening	31.66	67.79	757.1	192.58	0.1					
25	Jl. Ujung Bori	Morning	28.74	65.55	756.15	172.02	1.04	29.09	64.15	756.03	180.02	1.04
		Midday	29.94	62.05	755.97	186.02	0.97					
		Afternoon	29.24	64.45	755.95	189.02	1.13					
		Evening	28.44	64.55	756.05	173.02	1.02					
26	Jl. Rajawali	Morning	29.16	71.09	756.06	156.31	1.93	29.51	69.69	755.94	164.31	1.93
		Midday	30.36	67.59	755.88	170.31	1.86					
		Afternoon	29.66	69.99	755.86	173.31	2.02					
		Evening	28.86	70.09	755.96	157.31	1.91					
27	Jl. Sulawesi	Morning	28.65	81.1	756.08	215.2	1.91	29	79.7	755.96	223.2	1.91
		Midday	29.85	77.6	755.9	229.2	1.84					
		Afternoon	29.15	80	755.88	232.2	2					
		Evening	28.35	80.1	755.98	216.2	1.89					
28	Jl. Penghibur	Morning	28.87	65.94	755.57	171.85	2.31	29.22	64.54	755.45	179.85	2.31
		Midday	30.07	62.44	755.39	185.85	2.24					
		Afternoon	29.37	64.84	755.37	188.85	2.4					
		Evening	28.57	64.94	755.47	172.85	2.29					
29	Jl. Penghibur	Morning	30.26	60.42	757.79	159.89	2.64	30.61	59.02	757.67	167.89	2.64
		Midday	31.46	56.92	757.61	173.89	2.57					
		Afternoon	30.76	59.32	757.59	176.89	2.73					
		Evening	29.96	59.42	757.69	160.89	2.62					
30	Jl. Landak Lama	Morning	30.21	65.77	756.41	170.86	1.37	30.56	64.37	756.29	178.86	1.37

Predictive model development and comparison

Simple linear regression

The simple linear regression model using total vehicle volume produced an R^2 of 0.566 and an adjusted R^2 of 0.550. Under leave-one-out cross-validation (LOOCV), the model yielded an RMSE of 29.36 μg/m³, an MAE of 22.94 μg/m³, a cross-validated R^2 of 0.509, and an observed–predicted correlation of r = 0.715. These results indicate that traffic activity alone explained a substantial part of the point-level PM_{10} variation, but additional meteorological information was required to improve predictive performance

Multicollinearity assessment

Before multiple regression, total vehicle volume and relative humidity were assessed for multicollinearity. Both predictors had tolerance values of 0.700 and VIF values of 1.428, indicating no problematic multicollinearity under the applied thresholds (Kim, 2019). The two predictors therefore contributed sufficiently distinct information within the selected model.

Multiple linear regression

The multiple linear model combined total vehicle volume and relative humidity and produced an

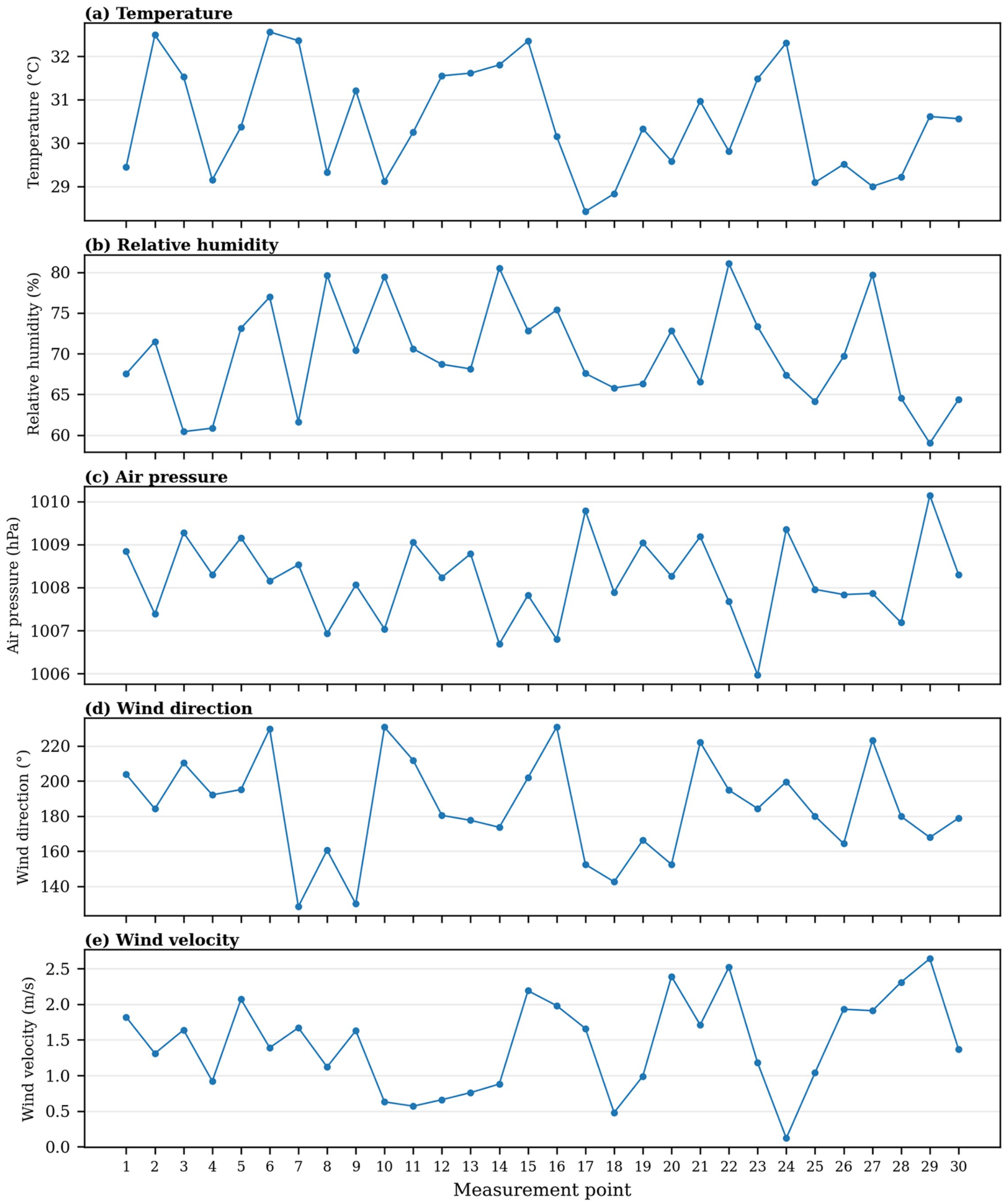

Figure 6. Meteorological conditions at the measurement points: (a) temperature, (b) relative humidity, (c) air pressure, (d) wind direction, and (e) wind velocity

Table 6. Shapiro–Wilk normality test results

Variable	p-value	Interpretation
PM_{10}	0.104	No significant departure from normality
Total vehicle volume	0.607	No significant departure from normality
Temperature	0.061	No significant departure from normality
Relative humidity	0.311	No significant departure from normality
Air pressure	0.969	No significant departure from normality
Wind direction	0.549	No significant departure from normality
Wind velocity	0.811	No significant departure from normality

Table 7. Pearson correlations with PM_{10} concentration

Variable	r	p-value	Interpretation
Total vehicle volume	0.752	1.65e-06	Strong positive
Relative humidity	-0.740	2.95e-06	Strong negative
Air pressure	0.730	4.72e-06	Strong positive
Wind direction	-0.150	0.429	Very weak negative
Temperature	0.100	0.599	Very weak positive
Wind velocity	-0.040	0.835	Very weak negative

R^2 of 0.720 and an adjusted R^2 of 0.699. Together, the predictors accounted for 72.0% of the variation in roadside PM_{10}. The selected model was:

$$PM_{10} = 352.822 + 0.004X_1 - 3.167X_2 \quad (13)$$

where: X_1 is total vehicle volume (vehicles/4 h) and X_2 is relative humidity (%).

The positive traffic coefficient indicates increasing PM_{10} with greater traffic activity when relative humidity is held constant. The negative humidity coefficient indicates decreasing PM_{10} as relative humidity increases when traffic volume is held constant. These coefficients describe associations within the observed dataset and are not universal causal effects (Table 8).

Both predictors remained statistically significant with HC3 robust inference. The standardized coefficients were similar in magnitude ($\beta = 0.495$ for total vehicle volume and $\beta = -0.469$ for relative humidity), indicating that both traffic activity and humidity contributed materially to the fitted model. The overall model was significant ($F = 34.635$, $p < 0.001$), with AIC = 277.086 and BIC = 281.290.

Exploratory fifth-order polynomial regression

Fifth-order polynomial regression was used as an exploratory traffic-only model to examine possible curvature in the relationship between total vehicle volume and PM_{10}. The fitted relationship was:

$$PM_{10} = 837.091 - 0.288928X + 4.37922 \times 10^{-5}X^2 - 3.08631 \times 10^{-9}X^3 + 1.05556 \times 10^{-13}X^4 - 1.41806 \times 10^{-18}X^5 \quad (14)$$

The polynomial model produced an R^2 of 0.626, which exceeded the simple linear model but remained below the multiple linear model. Its AIC (291.705) and BIC (300.112) were also higher than those of the MLR model. Under LOOCV, the polynomial model produced an RMSE of 30.18 μg/m³, an MAE of 23.67 μg/m³, and a cross-validated R^2 of 0.481. Thus, the additional mathematical flexibility did not improve out-of-sample performance and increased the risk of overfitting in the 30-point dataset. The model was therefore retained only as an exploratory nonlinear comparison (Figure 7).

Random Forest benchmark

Random Forest was evaluated as a nonlinear machine-learning benchmark using the same two predictors as the MLR model. Its fitted R^2 was 0.793, but LOOCV yielded an RMSE of 26.59 μg/m³, an MAE of 21.74 μg/m³, a cross-validated R^2 of 0.597, and an observed–predicted correlation of $r = 0.773$. Although the Random Forest provided a stronger in-sample fit, it did not outperform the MLR under cross-validation. This result supports retaining the MLR as the primary model because it combined the lowest cross-validated error with greater parsimony and direct coefficient interpretation. Random Forest should therefore be interpreted as a benchmark rather than evidence that machine-learning approaches are generally inferior.

Table 8. Statistical estimates for the selected multiple linear regression model

Predictor	B	SE	Standardized β	p-value	95% CI	HC3 p-value
Intercept	352.8225	67.5797	—	<0.001	214.1603 to 491.4846	<0.001
Total vehicle volume	0.004396	0.001081	0.495	<0.001	0.002179 to 0.006614	<0.001
Relative humidity	−3.166794	0.822559	−0.469	<0.001	−4.854546 to −1.479041	0.0039

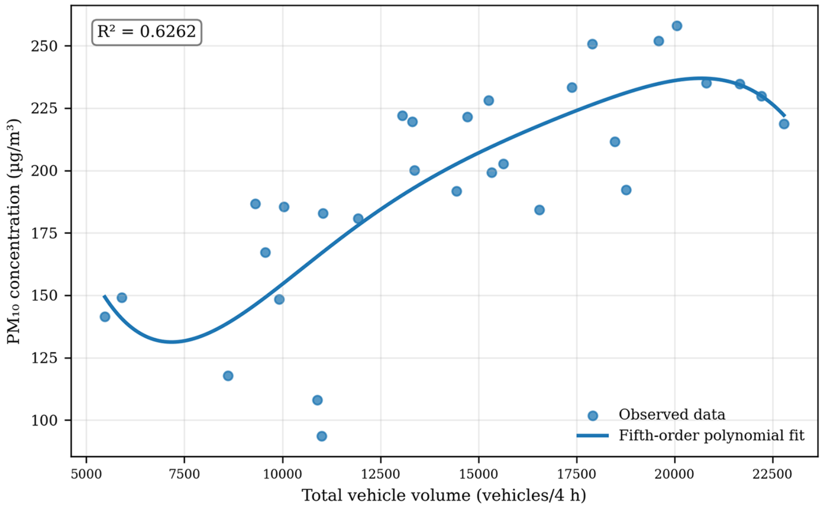

Figure 7. Exploratory fifth-order polynomial relationship between total vehicle volume and PM_{10} concentration

Model comparison and validation

Across the four approaches, the MLR produced the lowest LOOCV RMSE and MAE and the highest cross-validated R^2. Random Forest ranked second under internal validation, while the fifth-order polynomial performed worse than the simpler SLR under LOOCV despite its higher fitted R^2. These results indicate that incorporating relative humidity improved predictive consistency more effectively than simply increasing model flexibility (Table 9).

Residual robustness assessment

Diagnostic testing did not identify major violations of the selected MLR assumptions. The residual Shapiro–Wilk test was not significant ($W = 0.9468$, $p = 0.1388$). The Breusch–Pagan test ($LM = 1.6865$, $p = 0.4303$) and White test ($LM = 8.7230$, $p = 0.1206$) did not indicate significant heteroscedasticity. The Durbin–Watson statistic was 2.514, the maximum Cook's distance was 0.292, and the maximum leverage was 0.215. Together with the retained significance of both predictors under HC3 robust inference, these findings support the stability of the selected coefficient estimates within the available 30-point dataset (Table 10).

Spatial assessment of model-estimated PM_{10}

Spatial autocorrelation

Global Moran's I indicated no statistically significant spatial autocorrelation in the measured PM_{10} concentrations ($I = -0.0783$, permutation $p = 0.247$) or in the MLR residuals ($I = -0.0623$, permutation $p = 0.445$). The absence of significant residual spatial autocorrelation suggests that no strong global spatial structure remained

Table 9. Comparison and internal validation of PM_{10} models

Model	Predictor(s)	R^2	Adj. R^2	AIC	BIC	LOOCV RMSE	LOOCV MAE	CV R^2	r	Role
SLR	Total vehicle volume	0.566	0.550	288.214	291.016	29.36	22.94	0.509	0.715	Traffic-only baseline
MLR	Total vehicle volume + relative humidity	0.720	0.699	277.086	281.290	24.79	18.62	0.650	0.807	Selected model
Polynomial (order 5)	Total vehicle volume	0.626	0.548	291.705	300.112	30.18	23.67	0.481	0.700	Exploratory nonlinear comparison
Random Forest	Total vehicle volume + relative humidity	0.793	—	—	—	26.59	21.74	0.597	0.773	Nonlinear ML benchmark

Table 10. Residual and robustness diagnostics for the selected MLR model

Diagnostic	Statistic	p-value	Interpretation
Residual Shapiro–Wilk	W = 0.9468	0.1388	No significant departure from normality
Breusch–Pagan	LM = 1.6865	0.4303	No significant heteroscedasticity detected
White test	LM = 8.7230	0.1206	No significant heteroscedasticity detected
Durbin–Watson	2.5142	—	Reported as a residual diagnostic
Maximum Cook's distance	0.2919	—	No single observation dominated the fit
Maximum leverage	0.2152	—	Influence remained within the observed sample structure

in the unexplained component of the MLR under the applied spatial weighting scheme. This result does not establish spatial independence at every local scale, but it reduces concern that a strong omitted global spatial pattern was driving the regression residuals.

Exploratory IDW visualization and spatial validation

The selected MLR was applied to the 30 monitored points using the full-precision fitted coefficients. Model-estimated PM_{10} ranged from 133.96 μg/m³ at Point 22 to 249.63 μg/m³ at Point 3. These values were used as the point inputs for the final IDW surface. Because the purpose of this step was visualization rather than independent geostatistical forecasting, the map was interpreted as an exploratory representation of relative spatial tendencies among the monitored locations.

Candidate IDW powers of p = 1, p = 2, and p = 3 were screened using leave-one-location-out validation. The lowest error was obtained with p = 1, and this value was retained for the final visualization. Using p = 1, spatial validation against omitted measured PM_{10} values produced an RMSE of 45.54 μg/m³, an MAE of 36.86 μg/m³, a cross-validated R^2 of −0.182, and an observed–predicted correlation of r = −0.496. The negative cross-validated R^2 indicates weak predictive performance at omitted locations. Accordingly, the IDW surface should not be interpreted as a validated prediction of PM_{10} at unsampled roads (Figure 8).

Higher model-estimated PM_{10} generally occurred at locations with greater total vehicle volume and lower relative humidity, consistent with the directions of the MLR coefficients. However, the limited leave-one-location-out spatial performance indicates that the IDW surface should be used only to illustrate relative variation around the monitored points. It is not a substitute for direct measurements, continuous monitoring, or an independently validated city-wide spatial prediction model.

DISCUSSION

Traffic and meteorological controls on roadside PM_{10}

The results show that roadside PM_{10} in Makassar was not adequately characterized by traffic activity alone. Total vehicle volume exhibited a strong positive association with PM_{10} (r = 0.752), while relative humidity showed a similarly strong negative association (r = −0.740). The location with the highest traffic volume was not the location with the highest PM_{10} concentration, further indicating that source intensity

Table 11. Spatial autocorrelation and IDW validation results

Assessment	Statistic / setting	Result	Interpretation
Measured PM_{10} spatial autocorrelation	Moran's I; 999 permutations	I = −0.0783; p = 0.247	No significant global spatial autocorrelation
MLR residual spatial autocorrelation	Moran's I; 999 permutations	I = −0.0623; p = 0.445	No significant global residual spatial autocorrelation
IDW power selection	Candidate p = 1–3	p = 1 retained	Lowest leave-one-location-out error
IDW spatial validation	RMSE / MAE	45.54 / 36.86 μg/m³	High interpolation error at omitted locations
IDW spatial validation	CV R² / r	−0.182 / −0.496	Limited predictive skill; exploratory use only

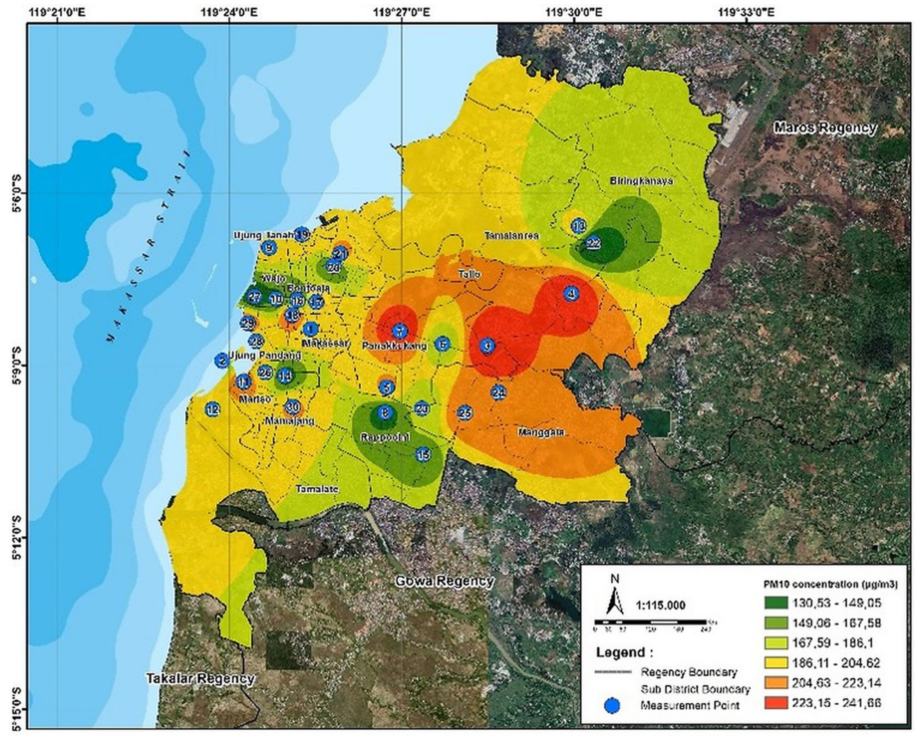

Figure 8. Exploratory spatial distribution of model-estimated PM_{10} concentrations using inverse distance weighting (IDW, p = 1)

and atmospheric conditions jointly shaped the observed point-level concentrations. This finding extends previous work in Makassar, where traffic-only linear and polynomial models described a substantial but incomplete fraction of PM_{10} variability (Aly et al., 2025). Comparable roadside studies have likewise shown that the relationship between traffic counts and particulate concentration can vary considerably because local meteorology and surrounding urban conditions modify dispersion, deposition, and accumulation (Lei and Ma, 2023).

The positive traffic association is environmentally plausible because road transport contributes particulate matter through both exhaust and non-exhaust processes, including brake and tire wear, pavement abrasion, and resuspension of deposited road dust. Non-exhaust sources can represent an important fraction of traffic-related particulate emissions, particularly where resuspension is enhanced by vehicle movement and road-surface conditions (Piscitello et al., 2021; Rienda and Alves, 2021). Accordingly, total vehicle volume should be interpreted as a practical indicator of overall traffic activity rather than as a direct measure of a single emission mechanism. The supplementary traffic-composition data improve reproducibility, but the present model intentionally retains total volume as the traffic predictor to avoid overparameterization with only 30 point-level observations.

Relative humidity contributed information beyond traffic volume. The negative association observed in Makassar is consistent with the possibility that higher moisture suppresses resuspension by increasing road-surface moisture and can favor particle deposition, although humidity–particle relationships are not universal and can vary with particle composition, climate, and atmospheric processes. Evidence from Jakarta has likewise demonstrated that meteorological influences on particulate pollution are complex and location dependent (Istiana et al., 2023). The strong positive bivariate association between PM_{10} and air pressure in the present dataset ($r = 0.730$) was therefore not interpreted as unimportant. Rather, air pressure was retained as a contextual meteorological correlate, while relative humidity was selected for the parsimonious two-predictor model because it had the largest absolute meteorological correlation and a more direct process-based interpretation for roadside particle deposition and resuspension. This modeling choice prioritizes interpretability and limits the number of predictors relative to the available sample size.

Model performance, comparison, and robustness

Adding relative humidity to the traffic-only model substantially improved explanatory and predictive performance. The simple linear model explained 56.6% of the observed PM_{10} variation, whereas the multiple linear model explained 72.0%. More importantly, the improvement persisted under leave-one-out cross-validation: MLR achieved the lowest RMSE (24.79 μg/m³) and MAE (18.62 μg/m³) and the highest cross-validated R^2 (0.650) among the evaluated approaches. The standardized coefficients of total vehicle volume (β = 0.495) and relative humidity (β = −0.469) were similar in absolute magnitude, indicating that both source activity and meteorological conditions contributed materially to the fitted relationship. Both predictors also remained statistically significant under HC3 robust inference, strengthening confidence that the coefficient interpretation was not driven solely by conventional standard-error assumptions (Mansournia et al., 2021).

The modern-model comparison is particularly important for evaluating whether the selected linear model was retained merely because of methodological simplicity. Random Forest produced a higher fitted R^2 (0.793), demonstrating greater flexibility in reproducing the observed sample, but its LOOCV performance was poorer than that of MLR (RMSE = 26.59 μg/m³; MAE = 21.74 μg/m³; CV R^2 = 0.597). Random Forests are capable of representing nonlinearities and interactions through ensembles of randomized trees (Scornet et al., 2015); however, with only 30 point-level observations, additional flexibility did not translate into superior internal predictive performance. The result should not be generalized to imply that Random Forest is inferior for PM_{10} prediction in larger datasets. Rather, within this dataset, the MLR provided the most favorable combination of cross-validated accuracy, parsimony, and direct environmental interpretability.

The fifth-order polynomial model provides a complementary warning about relying on in-sample fit alone. Although its fitted R^2 (0.626) exceeded that of SLR, its AIC and BIC were higher than those of MLR, and its LOOCV performance deteriorated to an RMSE of 30.18 μg/m³ and a CV R^2 of 0.481. This pattern is consistent with the broader principle that increasingly flexible predictive forms can capture sample-specific curvature without improving generalization. The polynomial model was therefore appropriately retained only as an exploratory nonlinear traffic-only comparison rather than as the final model.

Regression diagnostics did not reveal major instability in the selected MLR. Residual normality was not rejected, the Breusch–Pagan and White tests did not indicate significant heteroscedasticity, and the maximum Cook's distance (0.292) did not indicate that a single observation dominated the fitted relationship. These diagnostics do not remove uncertainty associated with the small sample, but together with HC3 inference and LOOCV they provide a more rigorous assessment than reliance on fitted R^2 alone. The resulting model is therefore best interpreted as an internally validated screening model for the monitored conditions, not as a universally transferable forecasting equation.

Spatial structure and the role of exploratory IDW visualization

The spatial analyses provide an important boundary on how far the point-level regression results can be generalized geographically. Global Moran's I was not statistically significant for either measured PM_{10} (I = −0.0783, p = 0.247) or the MLR residuals (I = −0.0623, p = 0.445). Moran's I is a global measure of spatial autocorrelation and is useful for determining whether neighboring observations collectively display clustering or dispersion beyond random expectation (Chen, 2023). In this study, the absence of significant residual spatial autocorrelation reduces concern that a strong global spatial pattern remained systematically unexplained by traffic volume and relative humidity. It does not, however, demonstrate spatial independence at every local scale or exclude localized effects associated with road geometry, land use, buildings, construction activity, or other nearby sources.

IDW was retained specifically as an exploratory visualization of model-estimated PM_{10} at the monitored locations. This distinction is important because deterministic interpolation can produce visually continuous surfaces even when predictive support between sampling points is weak. Previous particulate-matter studies have used IDW to display spatial patterns and have emphasized the value of validation when assessing interpolation performance (Shukla et al., 2020; Choi & Chong, 2022). In the present analysis, power values p =

1–3 were tested rather than selected arbitrarily, and p = 1 produced the lowest leave-one-location-out error. Nevertheless, the spatial validation remained weak (RMSE = 45.54 μg/m³; MAE = 36.86 μg/m³; CV $R^2 = -0.182$), indicating that the IDW surface cannot be considered a validated prediction for omitted or unsampled roads.

Consequently, the scientific value of the spatial component lies in showing relative spatial tendencies in the model-estimated values while explicitly quantifying the limits of interpolation. The map should not be read as a substitute for direct measurements or as evidence that concentrations between the 30 locations are known with high certainty. This restricted interpretation directly addresses the small spatial sample and avoids overextending a deterministic visualization into a city-wide forecasting claim.

Scientific contribution, implications, and study limitations

The principal contribution of this study is therefore not the use of a new regression or interpolation algorithm, but the demonstration—under a common 30-point roadside dataset—that meteorological information materially improves a traffic-only description of PM_{10}, that this improvement persists under internal cross-validation, and that a more flexible machine-learning benchmark does not automatically provide better generalization in a small dataset. The standardized MLR coefficients further show that traffic activity and relative humidity contributed at comparable magnitudes but in opposite directions. Together, these results refine the earlier traffic-centered understanding of roadside PM_{10} in Makassar and support an integrated source–meteorology interpretation rather than a single-factor explanation.

The study also has limitations that constrain generalization. Measurements covered selected one-hour periods and were aggregated to point-level means, so the dataset does not represent continuous 24-h, diurnal, or seasonal variability. The sample size of 30 points limits the complexity that can be estimated reliably and is insufficient for strong city-wide spatial prediction. Important local covariates—including detailed road-surface condition, intersection proximity, building density, green infrastructure, construction activity, and other nearby emission sources—were not incorporated in the final statistical model. In addition, validation was internal; no independent season, time period, city sector, or official monitoring-station dataset was available for external validation. These limitations explain why the regression is framed as a screening model and the IDW map as exploratory. Future investigations should prioritize repeated seasonal measurements and independent validation while recording additional roadside and urban-form covariates, but these needs do not alter the internally observed improvement obtained by integrating traffic volume with relative humidity.

CONCLUSIONS

This study demonstrates that roadside PM_{10} variability in Makassar is better explained by considering traffic activity together with meteorological conditions than by using traffic volume alone. Total vehicle volume showed a strong positive association with PM_{10}, whereas relative humidity showed a strong negative association, and their similar standardized effects indicate that both source intensity and atmospheric conditions were important within the monitored dataset. Incorporating relative humidity into the traffic-based model improved both explanatory performance and internal predictive consistency.

Among the evaluated approaches, the multiple linear regression model provided the best balance of predictive performance, parsimony, and interpretability. Its cross-validated performance exceeded the traffic-only linear model, the fifth-order polynomial model, and the Random Forest benchmark, while residual and robust-inference diagnostics did not indicate major instability. Thus, the scientific gain of the study lies in showing that additional model complexity alone did not outperform an environmentally informed, parsimonious specification in this 30-point dataset.

The spatial assessment further clarifies the scope of the findings. No significant global spatial autocorrelation was detected in measured PM_{10} or MLR residuals, while leave-one-location-out validation showed that IDW had limited predictive skill at omitted sites. Accordingly, the IDW surface is retained only as an exploratory representation of relative spatial tendencies and not as a validated city-wide concentration map. Overall, the study provides a reproducible, internally validated framework for interpreting roadside PM_{10} in Makassar while maintaining appropriately limited claims for temporal and spatial generalization.

Acknowledgements

The authors sincerely thank their academic advisors for their guidance, valuable input, and continuous support throughout this study. Appreciation is also extended to the Department of Environmental Engineering, Faculty of Engineering, University of Hasanuddin for providing the measurement instruments, laboratory facilities, and technical assistance required for the research. The authors are grateful to all parties involved in the field data collection and to their families and colleagues for their encouragement and support throughout the completion of this study.

REFERENCES

1. Aly, S. H., Harusi, N. M. R., Wah, Y. C., Handayani, A., Salsabila, P. H. (2025). Linear and polynomial regression analysis of the relationship between vehicle volume and PM_{10} concentration on road sections in Makassar City. *E3S Web of Conferences, 682*, 04005. https://doi.org/10.1051/e3sconf/202568204005
2. Badan Standardisasi Nasional. (2016). SNI 7119.15:2016: Ambient air—Part 15: Test method for particles with sizes ≤10 µm (PM_{10}) using High Volume Air Sampler equipment and the gravimetric method (in Indonesian). Badan Standardisasi Nasional.
3. Chaiprakarn, S., Kheawseema, P., Suten, U., Saengseedam, P. (2025). The influences of meteorological parameters on $PM_{2.5}$ and PM_{10} values in Rayong's pollution control zone, Thailand. *Ecological Engineering & Environmental Technology, 26*(12), 90–102. https://doi.org/10.12912/27197050/213680
4. Choi, K., Chong, K. (2022). Modified inverse distance weighting interpolation for particulate matter estimation and mapping. *Atmosphere, 13*(5), 846. https://doi.org/10.3390/atmos13050846
5. Dominski, F. H., Branco, J. H. L., Buonanno, G., Stabile, L., da Silva, M. G., Andrade, A. (2021). Effects of air pollution on health: A mapping review of systematic reviews and meta-analyses. *Environmental Research, 201*, 111487. https://doi.org/10.1016/j.envres.2021.111487
6. Government of the Republic of Indonesia. (2021). Government Regulation of the Republic of Indonesia Number 22 of 2021 concerning the implementation of environmental protection and management. Government of the Republic of Indonesia.
7. Harrison, R. M., Allan, J., Carruthers, D., Heal, M. R., Lewis, A. C., Marner, B., Murrells, T., & Williams, A. (2021). Non-exhaust vehicle emissions of particulate matter and volatile organic compounds from road traffic: A review. *Atmospheric Environment, 262*, 118592. https://doi.org/10.1016/j.atmosenv.2021.118592
8. Istiana, T., Kurniawan, B., Soekirno, S., Nahas, A., Wihono, A., Nuryanto, D. E., Adi, S. P., Hakim, M. L. (2023). Causality analysis of air quality and meteorological parameters for $PM_{2.5}$ characteristics determination: Evidence from Jakarta. *Aerosol and Air Quality Research, 23*, 230014. https://doi.org/10.4209/aaqr.230014
9. James, G., Witten, D., Hastie, T., Tibshirani, R. (2021). *An introduction to statistical learning: With applications in R (2nd ed.)*. Springer. https://doi.org/10.1007/978-1-0716-1418-1
10. Kim, J. H. (2019). Multicollinearity and misleading statistical results. *Korean Journal of Anesthesiology, 72*(6), 558–569. https://doi.org/10.4097/kja.19087
11. Laña, I., Del Ser, J., Padró, A., Vélez, M., Casanova-Mateo, C. (2016). The role of local urban traffic and meteorological conditions in air pollution: A data-based case study in Madrid, Spain. *Atmospheric Environment, 145*, 424–438. https://doi.org/10.1016/j.atmosenv.2016.09.052
12. Mishra, P., Pandey, C. M., Singh, U., Gupta, A., Sahu, C., Keshri, A. (2019). Descriptive statistics and normality tests for statistical data. *Annals of Cardiac Anaesthesia, 22*(1), 67–72. https://doi.org/10.4103/aca.ACA_157_18
13. Orellano, P., Reynoso, J., Quaranta, N., Bardach, A., Ciapponi, A. (2020). Short-term exposure to particulate matter (PM_{10} and $PM_{2.5}$), nitrogen dioxide, and ozone and all-cause and cause-specific mortality: Systematic review and meta-analysis. *Environment International, 142*, 105876. https://doi.org/10.1016/j.envint.2020.105876
14. Piscitello, A., Bianco, C., Casasso, A., Sethi, R. (2021). Non-exhaust traffic emissions: Sources, characterization, and mitigation measures. *Science of the Total Environment, 766*, 144440. https://doi.org/10.1016/j.scitotenv.2020.144440
15. Rienda, I. C., Alves, C. A. (2021). Road dust resuspension: A review. *Atmospheric Research, 261*, 105740. https://doi.org/10.1016/j.atmosres.2021.105740
16. Sahanavin, N., Prueksasit, T., Tantrakarnapa, K. (2018). Relationship between PM_{10} and $PM_{2.5}$ levels in high-traffic areas determined using path analysis and linear regression. *Journal of Environmental Sciences, 69*, 105–114. https://doi.org/10.1016/j.jes.2017.01.017
17. Savirah Nurul Auliah, M. A., Aly, S. H., Harusi, N. M. R. (2023). Analysis of NO_x, SO_2, PM_{10}, and CO emission loads from motorized vehicles at collector roads in Makassar City using the Tier 2 method. *IOP Conference Series: Earth and Environmental Science, 1272*(1), 012041. https://doi.

org/10.1088/1755-1315/1272/1/012041

18. Schober, P., Boer, C., Schwarte, L. A. (2018). Correlation coefficients: Appropriate use and interpretation. *Anesthesia & Analgesia, 126*(5), 1763–1768. https://doi.org/10.1213/ANE.0000000000002864
19. Taheri Shahraiyni, H., Sodoudi, S. (2016). Statistical modeling approaches for PM_{10} prediction in urban areas: A review of 21st-century studies. *Atmosphere, 7*(2), 15. https://doi.org/10.3390/atmos7020015
20. World Meteorological Organization. (2021). Guide to instruments and methods of observation (WMO-No. 8). World Meteorological Organization.
21. Scornet, E., Biau, G., Vert, J.-P. (2015). Consistency of random forests. The Annals *of Statistics, 43*(4), 1716–1741. https://doi.org/10.1214/15-AOS1321
22. Mansournia, M. A., Nazemipour, M., Naimi, A. I., Collins, G. S., & Campbell, M. J. (2021). Reflection on modern methods: Demystifying robust standard errors for epidemiologists. *International Journal of Epidemiology, 50*(1), 346–351. https://doi.org/10.1093/ije/dyaa260
23. Chen, Y. (2023). Spatial autocorrelation equation based on Moran's index. *Scientific Reports, 13*, 19296. https://doi.org/10.1038/s41598-023-45947-x
24. Shukla, K., Kumar, P., Mann, G. S., Khare, M. (2020). Mapping spatial distribution of particulate matter using Kriging and Inverse Distance Weighting at supersites of megacity Delhi. *Sustainable Cities and Society, 54*, 101997. https://doi.org/10.1016/j.scs.2019.101997